IOWA STATE UNIVERSITY
Digital Repository

Physics and Astronomy Publications | Physics and Astronomy

4-2006

Atomistic lattice-gas modeling of CO oxidation on Pd(100): Temperature-programed spectroscopy and steady-state behavior

Da-Jiang Liu
Ames Laboratory, dajiang@fi.ameslab.gov

James W. Evans
Iowa State University, evans@ameslab.gov

Follow this and additional works at: http://lib.dr.iastate.edu/physastro_pubs

 Part of the Biological and Chemical Physics Commons, and the Mathematics Commons

The complete bibliographic information for this item can be found at http://lib.dr.iastate.edu/physastro_pubs/201. For information on how to cite this item, please visit http://lib.dr.iastate.edu/howtocite.html.

This Article is brought to you for free and open access by the Physics and Astronomy at Iowa State University Digital Repository. It has been accepted for inclusion in Physics and Astronomy Publications by an authorized administrator of Iowa State University Digital Repository. For more information, please contact digirep@iastate.edu.

Atomistic lattice-gas modeling of CO oxidation on Pd(100): Temperature-programed spectroscopy and steady-state behavior

Abstract
We have developed an atomistic lattice-gas model for the catalytic oxidation of CO on single-crystal Pd(100) surfaces under ultrahigh vacuum conditions. This model necessarily incorporates an detailed description of adlayer ordering and adsorption-desorption kinetics both for CO on Pd(100), and for oxygen on Pd(100). Relevant energetic parameters are determined by comparing model predictions with experiment, together with some guidance from density functional theory calculations. The latter also facilitates description of the interaction and reaction of adsorbed CO and oxygen. Kinetic Monte Carlo simulations of this reaction model are performed to predict temperature- programed reaction spectra, as well as steady-state bifurcation behavior.

Keywords
adsorption-desorption kinetics, atomistic lattice-gas models, temperature-programmed spectroscopy, ultrahigh vacuum conditions, carbon monoxide, catalysis, desorption, mathematical models, Monte Carlo methods, oxidation, reaction kinetics, spectroscopic analysis, vacuum applications, crystal lattices

Disciplines
Biological and Chemical Physics | Mathematics

Comments
The following article appeared in *Journal of Chemical Physics* 124,15 (2006): 154705 and may be found at doi: 10.1063/1.2186314.

Rights
Copyright 2006 American Institute of Physics. This article may be downloaded for personal use only. Any other use requires prior permission of the author and the American Institute of Physics.

This article is available at Iowa State University Digital Repository: http://lib.dr.iastate.edu/physastro_pubs/201

AIP | The Journal of Chemical Physics

Atomistic lattice-gas modeling of CO oxidation on Pd(100): Temperature-programed spectroscopy and steady-state behavior

Da-Jiang Liu and J. W. Evans

Citation: The Journal of Chemical Physics **124**, 154705 (2006); doi: 10.1063/1.2186314
View online: http://dx.doi.org/10.1063/1.2186314
View Table of Contents: http://scitation.aip.org/content/aip/journal/jcp/124/15?ver=pdfcov
Published by the AIP Publishing

Articles you may be interested in

Transient and steady state CO oxidation kinetics on nanolithographically prepared supported Pd model catalysts: Experiments and simulations
J. Chem. Phys. **123**, 054701 (2005); 10.1063/1.1949167

Lattice-gas modeling of CO adlayers on Pd(100)
J. Chem. Phys. **121**, 4352 (2004); 10.1063/1.1778134

Metal nanoparticles as models of single crystal surfaces and supported catalysts: Density functional study of size effects for CO/Pd(111)
J. Chem. Phys. **117**, 9887 (2002); 10.1063/1.1516798

Reaction kinetics on supported model catalysts: Molecular beam/in situ time-resolved infrared reflection absorption spectroscopy study of the CO oxidation on alumina supported Pd particles
J. Vac. Sci. Technol. A **19**, 1516 (2001); 10.1116/1.1345910

The CO oxidation kinetics on supported Pd model catalysts: A molecular beam/in situ time-resolved infrared reflection absorption spectroscopy study
J. Chem. Phys. **114**, 4669 (2001); 10.1063/1.1342240

This article is copyrighted as indicated in the article. Reuse of AIP content is subject to the terms at: http://scitation.aip.org/termsconditions. Downloaded to IP: 129.186.176.40 On: Tue, 19 Jan 2016 22:18:43

Atomistic lattice-gas modeling of CO oxidation on Pd(100): Temperature-programed spectroscopy and steady-state behavior

Da-Jiang Liu[a)]
Ames Laboratory—U.S. Department of Energy, Iowa State University, Ames, Iowa 50011

J. W. Evans
Ames Laboratory—U.S. Department of Energy, Iowa State University, Ames, Iowa 50011
and Department of Mathematics, Iowa State University, Ames, Iowa 50011

(Received 7 September 2005; accepted 16 February 2006; published online 17 April 2006)

We have developed an atomistic lattice-gas model for the catalytic oxidation of CO on single-crystal Pd(100) surfaces under ultrahigh vacuum conditions. This model necessarily incorporates an detailed description of adlayer ordering and adsorption-desorption kinetics both for CO on Pd(100), and for oxygen on Pd(100). Relevant energetic parameters are determined by comparing model predictions with experiment, together with some guidance from density functional theory calculations. The latter also facilitates description of the interaction and reaction of adsorbed CO and oxygen. Kinetic Monte Carlo simulations of this reaction model are performed to predict temperature-programed reaction spectra, as well as steady-state bifurcation behavior. © *2006 American Institute of Physics*. [DOI: 10.1063/1.2186314]

I. INTRODUCTION

Traditionally, mean-field rate equations have been used for the analysis of chemical kinetics observed in heterogeneous catalytic reactions on metal surfaces under well-controlled ultrahigh vacuum (UHV) conditions.[1] While such analyses have been particularly instructive, it has long been recognized that the mean-field assumption of well-stirred spatially randomized reactants can break down due to adlayer ordering or islanding.[2] Such ordering occurs primarily as a result of adspecies interactions. In principle, atomistic lattice-gas (LG) modeling can provide a realistic description of such ordering, where LG model behavior can be determined precisely by Monte Carlo simulation. This approach has been applied extensively to single-species chemisorption systems, primarily to analyze phase transitions in adsorbate ordering,[3,4] and temperature-programed desorption (TPD) spectra.[5–7] In contrast, because of the greater complexity of catalytic surface reactions, realistic atomistic modeling of these processes is rare. This is the case even for basic reactions such as CO oxidation on low-index (100) and (111) single-crystal surfaces of such metals as Pt, Pd, or Rh.

There have, however, been significant recent advances in atomistic LG modeling incorporating energetic information based entirely on *ab initio* density functional theory (DFT). This approach has been applied to both TPD behavior for simpler systems,[8–10] and for surface reaction behavior in more complex systems.[11,12] When such models are analyzed by kinetic Monte Carlo (KMC) simulation, this approach is sometimes referred to as *ab initio* KMC. TPD studies have exploited *ab initio* energetics to describe adspecies interactions in terms of pair, triplet, etc., components,[8] as well as incorporating different types of adsorption sites.[9] Reaction studies have considered systems with complex many step mechanisms where adspecies are relatively disordered,[11] as well as high-pressure CO oxidation where strong chemical interactions rather than weak adspecies interactions dominate reaction kinetics.[12] For the latter, simultaneous activation of several reaction pathways can reduce the level of accuracy required in determination of individual activation barriers. In both cases, adlayer ordering is not a significant determinant of reaction behavior.

Our interest here is in CO oxidation under UHV conditions on well-characterized single-crystal surfaces. Compared with the above mentioned complex system, reaction is generally controlled in large part by a subtle cooperative effect, i.e., ordering of the mixed reactant adlayer. This ordering is in turn determined by and very sensitive to not just one but many weak adspecies interactions. It should be noted that such modeling must also appropriately treat the kinetics of adsorption-desorption. The latter impacts behavior of nonequilibrium reactive steady states and of temperature-programed reaction (just as it does for TPD behavior in simpler systems).

One could in principle apply *ab initio* KMC to model such systems. However, the current state of DFT theory is not adequate to reliably determine all of the relevant energetics, especially the weaker adspecies interactions. Thus, our approach is to develop an atomistic LG model based on an understanding of the most important features of the reaction system. Then, the key interactions and activation barriers are treated as free parameters. We use selected *ab initio* energetics as a guideline, while adjusting these important parameters to fit with experimental observations for adlayer ordering, TPD, etc. This approach has been criticized as based on effective parameters with possibly limited physical significance.[12] However, with an informed choice of model, currently this approach can often achieve better predictive

[a)]Electronic mail: dajiang@fi.ameslab.gov

 © 2006 American Institute of Physics

This article is copyrighted as indicated in the article. Reuse of AIP content is subject to the terms at: http://scitation.aip.org/termsconditions. Downloaded to IP: 129.186.176.40 On: Tue, 19 Jan 2016 22:18:43

capability than generic *ab initio* KMC. This is the case not just for reaction systems, but also for other processes such as thin film growth[13] where behavior is controlled by small barriers or weak interactions.

In this paper, we provide comprehensive atomistic modeling of CO oxidation on the Pd(100) surface under UHV conditions. We consider both steady-state behavior under simultaneous exposure of the catalyst surface to CO and oxygen, as well as temperature-programed reaction kinetics. Perhaps the most comparable previous study involved realistic modeling of CO oxidation on Pt(111).[14] This work analyzed titration of preadsorbed oxygen by exposure to CO, as well as TPD. Our choice of CO oxidation on Pd(100) is motivated by the fact that CO on Pd(100) and oxygen on Pd(100) constitute classic chemisorption systems (although analysis of these systems was quite incomplete until recently[15,16]). The Pd(100) substrate, like Pt(111), does not reconstruct during reaction, which simplifies our atomistic modeling. In the absence of surface reconstruction, CO oxidation is expected to constitute a classic bistable system.[1] At lower temperatures, a stable reactive state (with high oxygen coverage and low O coverage) can coexist with an inactive or near CO-poisoned state (with high CO coverage and low oxygen coverage). Bistability should disappear for temperatures above some critical value (i.e., a nonequilibrium critical point, which corresponds to a cusp bifurcation).

It is appropriate to mention here some additional previous investigations relevant to CO oxidation on Pd(100). A pioneering UHV study by Stuve *et al.*[17] provided detailed temperature-programed reaction (TPR) spectra, as well as some low energy electron diffraction (LEED) data for this system. Subsequent TPR work explored the reactivity of various surface oxygen phases on Pd(100) to CO, although mainly focusing on surface oxide phases associated with high oxygen exposures.[18] A recent study revealed a significant role of oxide formation during CO oxidation on Pd(100) at high pressure.[19] Our study considers only oxygen exposures below the threshold for surface oxide formation, although our model is a natural starting point for atomistic analysis of the high-pressure regime. Finally, there have also been recent DFT studies exploring specific aspects of this reaction.[20,21]

The outline of the paper is as follows. A detailed description of the various atomistic processes and interactions incorporated into our LG reaction model for CO oxidation on Pd(100) is presented in Sec. II. In addition, we describe our procedure for determination of relevant energetic parameters. In Sec. III, we briefly discuss some algorithmic issues pertaining to KMC simulation of the LG model. Before presenting results for the reaction of CO and oxygen on Pd(100), it is appropriate to review model predictions for adsorption and desorption of the individual reactants. As these individual processes are key components of CO oxidation, realistic behavior must obtained in order for the reaction model to be deemed reliable. Thus, we first present simulation results for the sticking coefficient and the TPD spectrum for CO on Pd(100) in Sec. IV. Corresponding results for oxygen are presented in Sec. V. Finally, our major simulation results for CO oxidation on Pd(100) are presented in Sec. VI. There are two main parts: determination of temperature-programed reaction (TPR) spectra and characterization of the steady-state bifurcation behavior (mapping out the regime of bistability).

II. LATTICE-GAS REACTION MODEL

A. Basic components of the LG model and parameter determination

Our lattice-gas reaction model is based on the standard Langmuir-Hinshelwood mechanism for CO oxidation on Pd(100). This mechanism includes the following steps.

(1) CO undergoes reversible molecular adsorption on the surface.
(2) O_2 undergoes dissociative adsorption on the surface (which is effectively irreversible under typical reaction conditions). Only atomic oxygen atoms and no molecular oxygen exists on the surface.
(3) Nearby adsorbed molecular CO and oxygen atoms react to produce the product CO_2 which immediately desorbs into the gas phase.

In this paper, we focus on the regime of chemisorption with no substrate reconstruction or oxide formation. Adsorbates reside on well-defined chemisorption sites of the (100) surface of fcc Pd, for which the surface lattice constant equals $a=2.75$ Å. For CO, adsorption sites are bridge (br), fourfold hollow (4fh), and on-top (top) sites. For O, only the 4fh sites can be occupied. Each site can accommodate only one adsorbate. In addition, we assume that adsorbates interact with pairwise-additive interactions which include an effective hard-core repulsion. [The hard-core interaction should generally depend on the types of the pair of adspecies under consideration. However, in our modeling for CO and O on Pd(100), we reasonably impose the requirement that no pair of any type can be separated by a distance of less than a.] We say that an adsorption site is *available* for adsorption if it is empty and if its occupancy does not incur any hard-core repulsion with its neighboring adsorbates.

In the following subsections, we discuss the details of the model together with our determination of key energetic parameters. As noted above, our general philosophy is to use DFT as a guide, but to choose parameters to recover selected experimental observations. Our previous preliminary modeling focused on matching adlayer ordering,[15,16,22] whereas the current study also considers TPD data. Our DFT studies were performed using the Vienna *ab initio* simulation package (VASP).[23,24] Unless noted otherwise, the generalized gradient approximation (GGA) with the Perdew-Burke-Ernzerhof (PBE) exchange-correlation functional[25] and the projector augmented wave (PAW) method[26] is used. Calculations were performed with four layer slab of Pd substrate using the theoretical equilibrium lattice constant of 3.96 Å (experiment 3.89 Å) separated by 16 Å of vacuum. The bottom two layers of Pd atoms were fixed at their bulk position, with the top two layers free to relax. Adsorbates were located on one side of the substrate. Calculations were also performed on five-layer-thick slab with no substrate relaxation, and with adsorbates on both sides of the slab. No significant differences were found between these different setups, and the differ-

This article is copyrighted as indicated in the article. Reuse of AIP content is subject to the terms at: http://scitation.aip.org/termsconditions. Downloaded to IP: 129.186.176.40 On: Tue, 19 Jan 2016 22:18:43

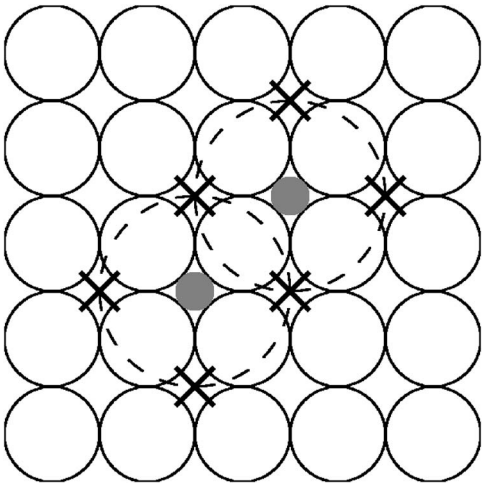

FIG. 1. Schematic for O_2 adsorption. The two grey circles represent O atoms. Crosses denote the six additional 4fh sites that should be free of O. The large circles with dashed line represent regions for which no CO should reside strictly within the interior.

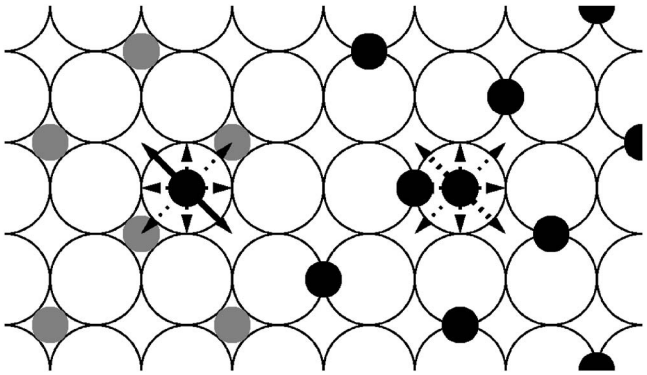

FIG. 2. Schematic for CO adsorption. CO molecule (black circle) is steered toward an on-top site. The arrows show the neighboring sites which it will check for the availability should the on-top site not be available for adsorption. The solid arrow indicates available adsorption sites and the dashed arrow indicates unavailable sites. On the left side, grey circles represent adsorbed oxygen which form a $c(2\times2)$ structure. On the right side, dark circles show adsorbed CO forming an ordered $c(2\sqrt{2}\times\sqrt{2})R45°$ domain. Inside this CO domain, no site is available for further CO adsorption.

ences in binding energies between one-side versus two-side adsorption are less than 20 meV. These observations are consistent with previously reported calculations.[20]

B. Adsorption of oxygen

O_2 molecules adsorb dissociatively on the Pd(100) surface with no molecular adsorption. The generic model for dissociative adsorption assumes that the diatomic can land on nearest-neighbor (NN) pair of empty adsorption sites.[27] However, it was argued that on various fcc(100) transition metal surfaces such as Ni(100)[28] and Pd(100),[16,29,30] oxygen adsorption follows a so-called "eight-site-ensemble" rule. Since there is a strong repulsion between oxygen adatoms on NN 4fh sites, the two adatoms formed by dissociative adsorption will occupy diagonal or next NN 4fh sites with separation $d=\sqrt{2}a$ (in contrast to the commonly assumed NN 4fh sites with separation $d=a$). Also due to the strong NN O–O repulsion, the six NN 4fh sites adjacent to the two adsorption sites (indicated by crosses in Fig. 1) must be free of oxygen for adsorption to occur, making a total of eight 4fh sites empty of O. These six NN 4fh sites need not necessarily be free of CO for oxygen adsorption. However, we do require that there should not be any CO *within* a distance a of either of the two adsorption sites.

Unlike CO described below, we assume that oxygen adatoms reside only at 4fh sites. DFT calculations with local density approximation (LDA) show that the binding energy at the bridge site is 0.90 eV higher than the hollow site, although with GGA, the difference is much smaller (e.g., 0.35 eV using the PBE exchange-correlation functional). Additional assessment of this energy difference also comes from the analysis of the diffusion barrier for O on Pd(100) which will be discussed in Sec. II E.

C. Adsorption of CO

Under common experimental conditions of low CO exposure, only bridge sites are found to be occupied for pure CO adsorption on Pd(100) surfaces.[31] However, other sites are occupied for higher exposure. Of particular relevance here is the feature that the occupation of 4fh sites also needs to be considered when CO is coadsorbed with oxygen. Since oxygen resides on 4fh sites and tends to form a checkerboard $c(2\times2)$ structure at higher coverages, CO–O repulsion (described in more detail below) tends to force CO into the remaining unoccupied 4fh sites. In addition, it has been argued[20] that during adsorption, CO is initially steered toward the on-top sites. DFT calculations with the PW91 exchange-correlation functional by Eichler and Hafner[20] using a $c(2\times2)$ unit cell with $\theta_{CO}=0.5$ ML indicate that the binding energy of CO at bridge, 4fh, and on-top sites are 1.92, 1.74, and 1.44 eV, respectively. However, DFT predictions of CO binding energy on metal surfaces are especially prone to errors.[32] In fact, using a $p(2\times2)$ unit cell with a lower coverage $\theta_{CO}=0.25$ ML, similar DFT-GGA calculations show that the bridge site and hollow site are almost degenerate. A recent study[33] with the DFT binding energy corrected through an extrapolation method predicts 1.641, 1.503, and 1.348 eV for bridge, 4fh, and on-top sites, respectively. Based on these various observations, in our LG model, we allow occupancy of CO at all three types of adsorption sites.

In this paper, we use a rather specific rule for CO adsorption, motivated by experiments[31,34,35] and DFT calculations.[20] A CO molecule in the gas phase is steered toward the on-top site. If the on-top site is available for adsorption, it will initially stick there. Otherwise it will first probe the four neighboring bridge sites. If any of these bridge sites is available, the CO molecule will adsorb there (and if more than one such site is available, one is chosen at random). If no such bridge site is available, it will then probe the four neighboring 4fh sites, and adsorb there if any is available. Figure 2 provides a schematic of this CO adsorption process. As can be seen from the figure, for this model, presence of oxygen adsorbates does not inhibit CO adsorption, even when they form a high-coverage $c(2\times2)$ struc-

This article is copyrighted as indicated in the article. Reuse of AIP content is subject to the terms at: http://scitation.aip.org/termsconditions. Downloaded to IP: 129.186.176.40 On: Tue, 19 Jan 2016 22:18:43

ture. On the other hand, a CO domain with perfect $c(2\sqrt{2}\times\sqrt{2})R45°$ ordering completely inhibits CO adsorption. We discuss this further in Sec. IV.

D. Adspecies interactions

We assume a Hamiltonian for the mixed adlayer system with the following form:

$$H = \sum_{i,\alpha} n_i^{\alpha}\epsilon_i^{\alpha} + \sum_{i<j}\sum_{\alpha,\beta} n_i^{\alpha} n_j^{\beta}\omega_{i,j}^{\alpha,\beta}, \tag{1}$$

where α and β=CO or O denote different possible adsorbed species, and i and j are the indices for the adsorption sites, which include br, 4fh, and top for CO (or just 4fh for O). Here, we assume that pairwise-additive interaction dominates adlayer ordering and reaction behavior. However, many-body interactions[8,10] also play some role, and could be readily be incorporated into a more detailed LG treatment. Furthermore, we allow for the dependence of the binding energy ϵ_i^{α} and the pair interaction $\omega_{i,j}^{\alpha,\beta}$ on the adsorption sites.

DFT provides a very useful tool for estimating lateral interactions between adsorbates. However, current accuracies, which are assumed to be around 50 meV, often are not sufficient to predict the correct equilibrium adlayer ordering. The latter requires uncertainties significantly below the thermal energy, k_BT, of about 25–40 meV for typical reaction temperatures of around 300–450 K. Hence, in this paper, we adopt a multifaceted approach in "deriving" the lateral interactions. We first studied the equilibrium phase diagrams for single-species adsorbate ordering in the appropriate temperature range. For CO, the relevant ordering is $c(2\sqrt{2}\times\sqrt{2})R45°$. For oxygen, the relevant ordering is (2×2) or $c(2\times2)$. Comparing phase diagrams from statistical mechanical analysis of the lattice-gas model and from experiment, we can place some constraints on the possible magnitudes of interactions. Some of these analyses has been reported previously.[15,16] In this work, our choice of interactions is also guided by the requirement of obtaining reasonable TPD spectra. Since different experimentally measurable quantities are sensitive to different interactions, modeling variety of such observations can effectively narrow down the range of viable interaction values. In addition, results from DFT calculations reported below further narrows down the range of possibilities. Our choice of parameters can reasonably reproduce all available experimental data, and also fall within the recognized uncertainties of current first-principles methods. Finally, we note that the "deduced" parameters cannot be the final answer, since adspecies interactions cannot be precisely described by pairwise interactions in the form of Eq. (1). However, we believe that our model, which can be considered as semiempirical, captures the dominant behavior.

Table I summarizes the lateral interactions between CO and O adsorbates. DFT calculations were performed with squared (1×1), $c(2\times2)$, (2×2), and (3×3) supercells, with Brillouin-zone integration using $(12\times12\times1)$, $(8\times8\times1)$, $(6\times6\times1)$, and $(4\times4\times1)$ **k** points, respectively. The cutoff energy for all atoms is 400 eV. To derive the lateral interaction from DFT calculations, we compare the binding energy per adsorbate from calculations with different periodic adlayer orderings and coverages. We assume additive pairwise interactions as in the lattice-gas Hamiltonian in Eq. (1), and ignore interactions for separations beyond $d=2a$. Then, the difference in binding energy between a 1 ML (1×1) and a 1/2 ML $c(2\times2)$ system corresponds to two NN interactions per adsorbate, and therefore the strength of NN interaction $\omega_{NN}=[E_b(1/2\ \text{ML})-E_b(1\ \text{ML})]/2$. Alternatively, one can also calculate ω_{NN} by comparing the difference in binding energy between an isolated adsorbate and a single NN pair. For the NN repulsion between two oxygen in hollow sites, the former method predicts a value of 0.36 eV, while the second method [performed using a (3×3) supercell] predicts a value of 0.38 eV. This supports the adequacy of the pairwise-additive interaction approximation. Since we are mostly interested in systems with coverages near or above that of ordered structures, we use the first method for deriving lateral interactions. [As an aside, comparing energies between a 1/4 ML (2×2) system and a 1/2 ML (2×1) system predicts a 0.52 eV NN repulsion, perhaps due to a strong orientational dependence in lateral interaction. Fortunately, such (2×1) ordering is highly energetically unfavorable, therefore accurate treatment is not required.]

TABLE I. Lateral interactions between CO and oxygen adsorbates. The first column indicates the site separation, d, in units of a. The second column indicates the adsorption sites for each of the two interacting adspecies, where "4fh" denotes fourfold hollow, "top" denotes on-top, and "br" denotes bridge sites. There are two br-br pairs with $d=a$: "br-br (1)" is across a 4fh site, and "br-br (2)" is across a Pd atom. Energies are in unit of eV.

$d(a)$	Adsorption sites	DFT values	Value used
	CO–CO		
1	4fh-4fh	0.408	0.408
1	br-br (1)	0.221	0.170
1	br-br (2)	0.304	0.170
$\sqrt{5}/2$	br-4fh	0.174	0.174
$\sqrt{5}/2$	br-top	0.078	0.174
$\sqrt{2}$	br-br	0.020	0.030
	O–O		
1	4fh-4fh	0.368	0.360
$\sqrt{2}$	4fh-4fh	0.104	0.085
2	4fh-4fh	−0.041	−0.020
	CO–O		
1	4fh-4fh	0.426	0.326
$\sqrt{5}/2$	br-4fh	0.200	0.190
$\sqrt{2}$	4fh-4fh	0.087	0.000

Note that many of the values for interaction energies used in the model are different from the DFT values also listed in Table I. For example, we deduce[15] from experiments[31,36,37] on the heat of adsorption that the interaction between two bridge site CO molecules at a distance of a to be 0.17 eV, rather than a value in the range of 0.22–0.30 eV obtained from DFT calculations.

E. Diffusion of adsorbates

At low to moderate coverages, by far the most prevalent and rapid process is the diffusive hopping of CO across the

This article is copyrighted as indicated in the article. Reuse of AIP content is subject to the terms at: http://scitation.aip.org/termsconditions. Downloaded to IP: 129.186.176.40 On: Tue, 19 Jan 2016 22:18:43

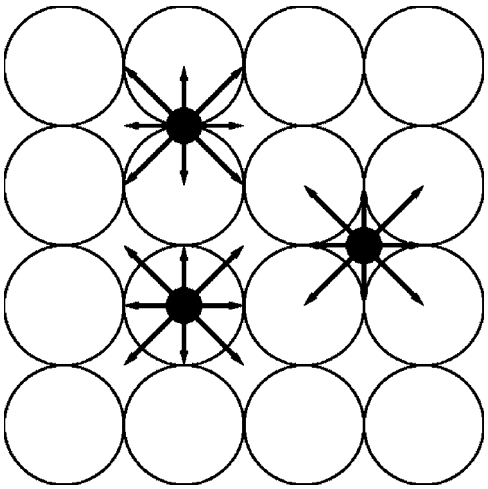

FIG. 3. Schematic indicating allowed CO hopping paths.

surface. Even the rate of hopping of relatively immobile O will exceed rates for other adsorption, desorption, and reaction processes at 300 K and above. A kinetic model that precisely describes all hopping processes is beyond the scope of this paper, but in any case is rather unnecessary. The main effect of diffusion is to achieve some degree of equilibration of the adlayer. This can be achieved by any kinetic model that treats diffusion in a way that satisfies detailed balance and ergodicity. In this paper, we use a simple Metropolis dynamics (or algorithm) where the hopping rate for adspecies of type α is given by

$$h = h_0^\alpha \min\{1, e^{(E_i - E_f)/(k_B T)}\}. \tag{2}$$

Here, E_i (E_f) is the total initial (final) adspecies interaction energy for this adsorbate before (after) hopping. h_0^α is a reference hopping rate (described further below) which is assumed to have the Arrhenius form

$$h_0^\alpha = \nu^\alpha \exp[-E_0^\alpha/(k_B T)], \tag{3}$$

where $\nu = 10^{13}$ s^{-1} for both CO and oxygen.

This form for h is certainly an oversimplification. It has the property that the hopping rate is independent of the lateral interactions as long as the hopping movement does not raise the energy. In general, one might expect that the hopping rate for adsorbate diffusion will increase to some extent with an increase in E_i, as evidenced in experiments on the hopping of O on Ru(0001).[38] However, again, here we deal primarily with the regime of rapid diffusion, where the main impact of diffusion is adlayer equilibration, and where the details of the diffusion dynamics are not so important.

Since CO can reside on different types adsorption sites, we allow hopping between them. For example, a CO(ads) on a bridge site can hop to any of the four NN bridge sites, the two NN 4fh sites, or the two NN on-top sites (if available). Figure 3 illustrates all of the possibilities. In contrast, O(ads) can only reside at 4fh sites, and is only allowed to hop to any of four NN 4fh sites (if available).

For oxygen (α=O), which occupies only 4fh sites, h_0^O corresponds to the rate of hopping between NN 4fh sites for an isolated O adatom. We choose a hopping barrier for oxygen of $E_0^O = E_d^O = 0.65$ eV. This choice is based on a detailed analysis of LEED experiments characterizing the nonequilibrium ordering dynamics of O/Pd(100).[16,29] As an aside, we note that this value should correspond to the difference in binding energy between bridge and 4fh sites.

For CO (α=CO), because we allow direct hops between the lowest energy bridge sites (which can lead to long-range diffusion), it follows that $E_0^{CO} = E_d^{CO}$ eV must be chosen to correspond to the diffusion barrier for isolated CO. (As an aside, if one forbids direct hops between bridge sites, then the dominant pathway for long-range diffusion presumably corresponds to hopping between neighboring bridge sites via the intervening 4fh site. In this case, the activation barrier for long-range diffusion of CO, E_d^{CO}, must satisfy $E_d^{CO} = E_0^{CO} + \delta^{CO}$, where $\delta^{CO} = \epsilon_{4fh}^{CO} - \epsilon_{br}^{CO}$.) In any case, this difference in site energies, δ^{CO}, undoubtedly provides a lower bound on E_d^{CO} for the real system. This δ^{CO} was estimated as 0.18 eV from DFT studies in Ref. 20, but was found to be significantly lower in our analysis (although a value of 0.18 eV is used in our modeling, as noted below). A recent more detailed analysis[33] suggests that $\delta^{CO} = 0.14$ eV, and our DFT results suggest an additional barrier of around 0.1 eV for diffusion corresponding to E_d^{CO} in the range of 0.20–0.25 eV.

However, since we deal with situations where CO diffusion is very fast, its precise value is not particularly relevant. In fact, in our simulations, we slow down CO diffusion significantly from its physical value (and sometimes also oxygen diffusion). We have checked that the results presented in this paper are mostly insensitive to the values of these diffusion rates. See Sec. III and the Appendix for further discussion.

F. Desorption of O

Desorption of oxygen is associative or recombinative, i.e., of second order. The desorption pathway starts from a diagonal NN pair of oxygen adatoms on 4fh sites. Rates for the oxygen adsorption-desorption process must satisfy detailed balance. Since we assume no barrier for dissociative adsorption of oxygen (just requiring satisfaction of the site availability condition), the rate for the reverse process of associative desorption must satisfy

$$d_{O_2} = \nu_{O_2} \exp[-(\epsilon^{O_2} + E_{lat}^{O_2})/(k_B T)]. \tag{4}$$

Here, ϵ^{O_2} is the adsorption energy of a O_2 molecule, i.e., the difference in energy between O_2 in the gas phase and two isolated O adsorbed at 4fh sites on the Pd(100) surface. $E_{lat}^{O_2}$ is the total lateral interaction for the pair of desorbing O with the rest of the coadsorbate, *including* the interaction between this pair of adsorbed O of $\omega_{i,j}^{O,O}$ where $\{i,j\}$ correspond to a diagonal NN pair of 4fh sites.

In our model, we assume $\nu_{O_2} = 10^{13}$ s^{-1}. Fitting to experimental TPD spectra (see below) so that the main desorption peak is at 800 K with heating rate of 5 K/s and an initial coverage of 0.15 ML gives $\epsilon^{O_2} = 2.25$ eV. A DFT calculation without spin polarization predicts that $\epsilon^{O_2} = 3.43$ eV. Better agreement with the experiment can be achieved by consider-

This article is copyrighted as indicated in the article. Reuse of AIP content is subject to the terms at: http://scitation.aip.org/termsconditions. Downloaded to IP: 129.186.176.40 On: Tue, 19 Jan 2016 22:18:43

ing spin polarization for O_2 molecule (but still assuming no spin polarization for the adsorption system), which yields the prediction $\epsilon^{O_2}=2.33$ eV.

G. Desorption of CO

Rates for the CO adsorption-desorption process must also satisfy detailed balance. Since we assume no barrier for CO adsorption (just requiring satisfaction of the site availability condition), the rate for the reverse process of CO desorption from site i must be given by

$$d_{CO} = \nu_{CO} \exp[-(\epsilon_i^{CO} + E_{lat}^{CO})/(k_B T)], \quad (5)$$

where ϵ_i^{CO} is the binding energy of an isolated CO on site i and E_{lat}^{CO} is the total lateral interaction of this CO with its neighboring adsorbates. In this paper, we assume that $\nu_{CO}=10^{16}$ s^{-1}, a value taken from experiments by Behm *et al.*[31] This choice is significantly larger than the canonical preexponential factor of 10^{13} s^{-1}, however, it has been argued[39] to be reasonable for CO desorption from metal surfaces. We also assume that $\epsilon^{CO}=1.60$ eV for the bridge site, $\epsilon^{CO}=1.42$ eV for the 4fh site, and $\epsilon^{CO}=1.13$ eV for the on-top site.

H. Reaction of CO and O

DFT calculations by Zhang and Hu[21] show that the activation barrier for the CO oxidation reaction on Pd(100) is about 1.05 eV in a 2×3 unit cell with 1/6 ML coverage of each of O and CO, and about 0.78 eV in a unit cell of 2×2 with 1/4 ML coverage of each of O and CO. In the former case, the O is initially at a 4fh site and the CO at the closest available bridge site ($d=1.118a$) or a next NN 4fh site ($d=1.414a$). These are the typical reaction configurations for lower adlayer coverages, and in our modeling we assume that a CO–O pair with these configurations can react with an activation barrier of 1.00 eV. In the later case, the O and CO are both on NN 4fh sites separated by a shorter distance a. This scenario applies for CO oxidation when the oxygen coverage is high. Then, this alternative reaction pathway becomes significant. The lower activation barrier is presumably due to the higher initial energy associated with the higher local coverage. In our modeling, we assume an activation barrier of 0.73 eV for this reaction pathway. Figure 4 provides a schematic of both pathways.

Note that the above choice of activation barriers for reaction is insensitive to the initial configurational energy which incorporates lateral interactions. Thus, for example, the reaction barrier for CO at a bridge sites inside a $p(2\times2)$ oxygen domain is the same as for CO at a bridge site outside of the domain but close to the edge. For reaction, there are no constraints imposed by detailed-balance requirements since the reverse process of dissociative adsorption of CO_2 is not included in the model. Thus, there is considerable flexibility in the choice of rates. Analogous to our imposition of Metropolis dynamics in Eq. (2) for hopping, our choice for reaction is certainly an oversimplification. Other possibilities incorporate the effect of interactions in the initial configuration, e.g., to lower the barrier for CO at bridge sites within oxygen $p(2\times2)$ domains (relative to CO outside such domains). However, as we will show in Sec. VI B, our model can reproduce TPR features that are associated with oxygen islanding.

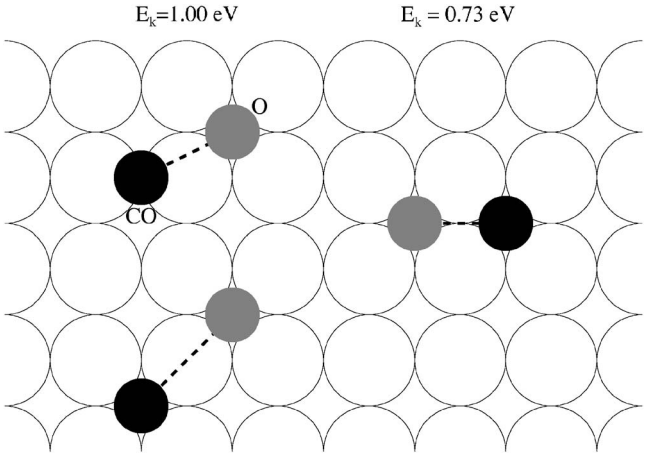

FIG. 4. Schematic of the two CO+O reaction pathways.

III. KEY FEATURES OF THE KMC SIMULATION ALGORITHM

Because of the complexity of our LG reaction model, a fully rejection-free Bortz-type algorithm is impractical to implement. Also, due to the vast range of dynamical rates for the various atomistic processes, a "standard" algorithm where the sites are randomly selected is extremely inefficient. Thus, we implement a tailored algorithm to accommodate these difficulties.

We maintain individual lists of CO adspecies and O adatoms on the various types of adsorption sites, i.e., CO on top sites, CO on 4fh sites, CO on bridges sites (in fact, we distinguish between two types of such sites, one between Pd aligned along the x direction and the other between Pd aligned along the y direction), and O on 4fh sites. In our simulations, we first determine the highest possible rate for each process, e.g., hopping of a bridge CO to a neighboring bridge sites, reaction between a bridge CO and a neighboring 4fh O, etc., based on the current configuration. We use these values as the reference or *attempt* rates for the various processes (for a certain period of time, as described below). Then, at each Monte Carlo step, a process is then selected based on the above mentioned lists weighted by the attempt rates. The probability for successful implementation of this process is given by the ratio of its actual rate to the maximal attempt rate.

It should be noted that for such activated processes as desorption of CO and O, there can be a great variation in the associated rates (reflecting variations in the local lateral interaction energetics). Thus, the acceptance rate can vary from unity to very low values. For adspecies hopping, the dependence of rates on lateral interactions also results in considerable variation in the acceptance rate. Adsorption processes must be treated appropriately along with desorption, reaction, and hopping. We do not keep lists of available adsorption sites, so acceptance depends whether or not the selected site (or sites in the case of O_2 adsorption) is available.

This article is copyrighted as indicated in the article. Reuse of AIP content is subject to the terms at: http://scitation.aip.org/termsconditions. Downloaded to IP: 129.186.176.40 On: Tue, 19 Jan 2016 22:18:43

Returning to the determination of reference or attempt rates, we indicated above that these are not determined continuously throughout the simulation. Rather, they are determined from some current configuration and then used for a certain interval of time. At the end of that interval, they are recalculated based on the updated current configuration. Strictly speaking, there *can* and *will* be cases where the "real" rate is larger than the reference rate thus determined. Consequently, we are possibly capping rates for these faster processes by the reference rates, effectively slowing down these processes slightly. However, if one updates the reference rates frequently enough, capping occurs rarely and will not corrupt the verity of the simulation.

Another issue particular to surface reaction systems is that adspecies diffusion is usually by far the fastest process. If we simulate diffusion processes using their physical rates (particularly for CO), this would consume almost all of the computational resources. However, since we consider only spatially homogeneous systems, as noted above, the effect of diffusion is primarily to equilibrate the system. Thus, behavior is typically insensitive to the exact magnitude of hopping rates provided that they are sufficiently large. Thus, in this paper, we typically cap the hopping rates of CO and O (by reducing the reference hopping rates, h_0^α) to be 10–100 times the fastest rate for the other processes, irrespective of whether it will be associated with reaction, deposition, etc. This approach significantly reduces rates for CO hopping, but not necessarily for O hopping (which is subject to much higher barriers). This has the advantage of preserving a realistic description of reordering dynamics of the O adlayer, e.g., during TPR.

An alternative strategy is to use an "artificial dynamics," at least for CO, to more efficiently equilibrate the system (e.g., with longer range hopping or artificial desorption readsorption using the Metropolis dynamics). However, due to the high coverage and strong repulsive interactions between adsorbate, such dynamics is highly restrained and no significant speedup is achieved. We are, however, pursuing the use of a cluster-type algorithm in a more general surface reaction studies.

As an aside, we note that for spatially inhomogeneous behavior in these reaction-diffusion systems, the characteristic length is proportional to the square root of the chemical diffusion coefficient for the most mobile species. Thus, reducing hop rates corrupts description of spatiotemporal behavior (which might be corrected by rescaling). However, we have also developed a heterogeneous coupled lattice-gas (HCLG) multiscale simulation approach for surface reactions.[22,40] Here, parallel simulations of the local state of the reaction system at a grid of macroscopic points across the pattern are suitably coupled to reflect macroscopic transport by surface diffusion.

IV. SIMULATION RESULTS FOR ADSORPTION AND DESORPTION OF CO

Figure 5 presents our simulation results for the coverage dependence of the normalized sticking coefficient, $S_{CO}(\theta_{CO})$, for CO adsorption on Pd(100). One caveat is that these results are specific to the steering mechanism for CO adsorption described in detail in Sec. II C. The most salient feature is that the sticking coefficient remains very close to unity for CO coverages up to at least 0.2 ML. This contrasts conventional linearly decreasing behavior with increasing CO coverage, as predicted by the Langmuir model for monomer adsorption. A slow or negligible initial decrease is a common phenomena in chemisorption systems, and is most typically attributed to existence of a physisorbed precursor state,[41] although it has also been recognized that this behavior can reflect a steering mechanism being operative.[42]

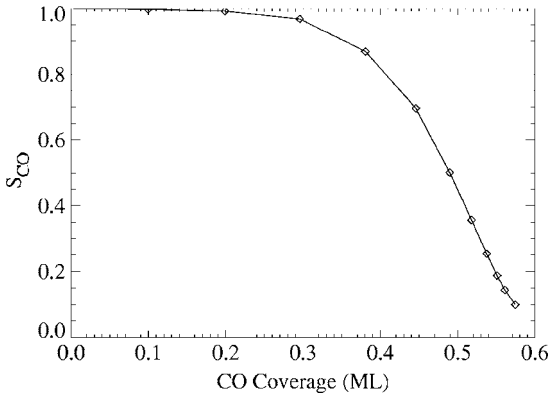

FIG. 5. Normalized sticking coefficient for CO adsorption at 300 K with impingement rate 1 ML/s.

For our model, the initial slow decrease of $S_{CO}(\theta_{CO})$ with increasing θ_{CO} is due to the steering effect. At low coverages, preadsorbed CO will steer an incoming gas-phase CO to a nearby adsorption site, rather than block the adsorption as in the normal Langmuir model of adsorption. As the CO coverage increases to about 0.5 ML, such a steering is no longer possible, since most nearby sites which can accommodate additional CO adsorption are already filled, as it is shown in Fig. 2. Therefore, the sticking coefficient decreases sharply around 0.5 ML.

Figure 6 shows simulation results for TPD spectra obtained with a heating rate of 13 K/s. The initial configuration is generated from simulated configurations obtained immediately following the deposition of various amounts of CO at two different temperatures, T_{dep}: (a) $T_{dep}=250$ K and (b) $T_{dep}=350$ K. The impingement rate was 2×10^{-3} per Pd(100) lattice site per second, taking the initial sticking coefficient equal to unity. This corresponds to a CO pressure of about 10^{-7} torr. The coverage of CO obtained under these conditions for an exposure of 1 L (1 L$=10^{-6}$ torr s) is about 0.53 ML for $T_{exp}=250$ K, and 0.44 ML for $T_{exp}=350$ K. Here, for modeling purposes, we define 1 L as the amount of exposure to cover the surface with 1 ML of CO if every incoming molecule sticks to the surface. (Later for O_2 adsorption, only a dose of 0.5 L is needed to cover the surface with 1 ML of oxygen if every molecule sticks, since each O_2 produces two atomic O.)

The dominant peak in our TPD spectra at 490 K agrees with experiments by Behm *et al.*[31] This should be expected since we have used a desorption prefactor $\nu_{CO}=10^{16}$ s^{-1} and binding energy $\epsilon_{br}^{CO}=1.60$ eV taken from that study. Deconvolution of the spectra would produce a secondary peak at

This article is copyrighted as indicated in the article. Reuse of AIP content is subject to the terms at: http://scitation.aip.org/termsconditions. Downloaded to IP: 129.186.176.40 On: Tue, 19 Jan 2016 22:18:43

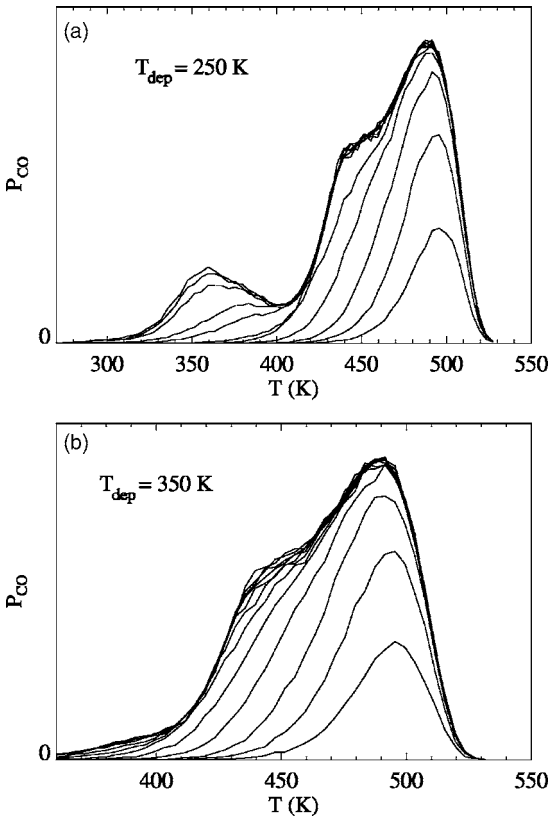

FIG. 6. Simulated TPD spectrum for CO desorption on Pd(100) for various CO exposures at (a) 250 K and (b) 350 K. Exposures are at 0.1, 0.2, 0.3, 0.4, 0.5, 0.6, 0.7, 0.8, 1.0, 1.2, 1.6, and 2.0 L, assuming an initial sticking coefficient of unity. Simulations are performed on a 512×512 system. The CO hopping rate is at least 100 times the desorption rate of an isolated CO at bridge sites.

about 440 K. This peak reflects enhanced desorption due to the weak second NN CO(br)–CO(br) repulsion ($d=\sqrt{2}a$) within $c(2\sqrt{2}\times\sqrt{2})R45°$ domains. When the surface is exposed to CO at a lower temperature, there is an additional peak at 360 K (as well as the main 490 K peak and the secondary 440 K peak). Behm *et al.* also mentioned a peak at 370 K in their experiments.[31] The same feature appears in TPD spectra of Stuve *et al.*[17] following adsorption at 125 K. In our model, this additional low temperature peak is due to the greatly reduced desorption barrier for CO molecules within high-density boundaries between different $c(2\sqrt{2}\times\sqrt{2})R45°$ domains. The barrier for such adspecies is reduced due to the strong NN CO(br)–CO(br) repulsion. Figure 7 shows a snapshot, a configuration generated in the TPD simulation when the system is at 360 K, with initial CO adsorption at 250 K.

As indicated above, TPD spectra can be quite sensitive to the lateral adspecies interactions, and, in fact, can be used to deduce these interactions (e.g., see Ref. 7). In our modeling, we used a NN CO(br)–CO(br) repulsion of 0.17 eV deduced from the heat of adsorption experiments.[15] This generates a 360 K TPD peak as shown above. In contrast, if one uses the higher DFT values for the NN CO(br)–CO(br) repulsion listed in Table I, this low temperature peak is shifted to near 320 K, too low to be consistent with the experiment. Therefore, the location of this peak in the TPD spectrum

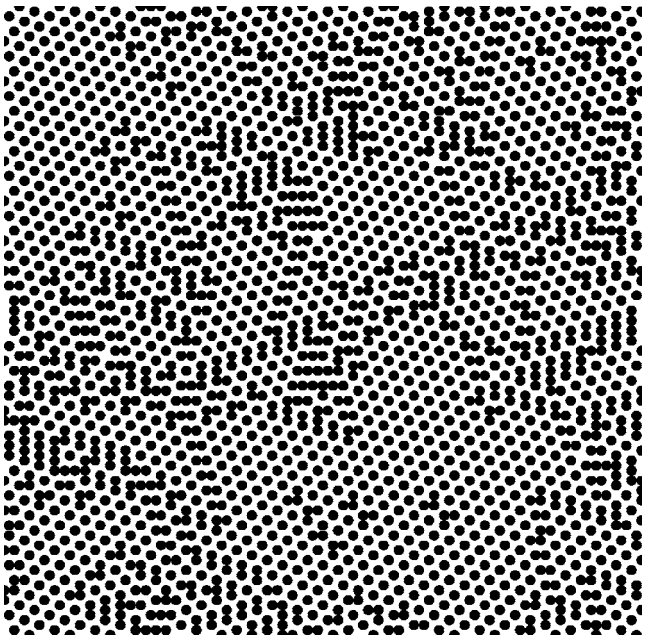

FIG. 7. Snapshot of the the configuration of CO adsorbates at 360 K during a TPD simulation. The surface was initially exposed to 2 L of CO at 250 K.

gives additional evidence that our lower value of 0.17 eV provides a better description of this CO NN repulsion.

V. SIMULATION RESULTS FOR ADSORPTION AND DESORPTION OF OXYGEN

Figure 8 shows simulation results for coverage dependence of the normalized sticking coefficient, $S_{O_2}(\theta_{O_2})$, for oxygen adsorption on Pd(100) at various temperatures (from 300 to 500 K). At these temperatures, diffusion of adsorbed oxygen is activated. When the oxygen coverage approaches 0.25 ML, $p(2\times2)$ ordering emerges and the sticking coefficient decreases sharply. This reflects the feature that the population of eight-site adsorption ensembles vanishes for such ordering. While the behavior of the sticking coefficient for lower coverages is only weakly dependent of temperature and pressure in this regime, there is a strong dependence for behavior near saturation.

We should mention a few caveats regarding these simulation results. First, the "eight-site rule" undoubtedly pro-

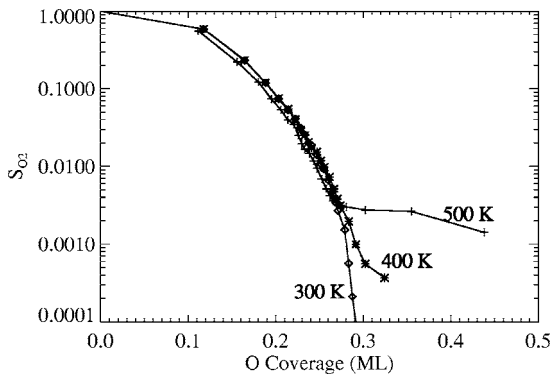

FIG. 8. Normalized sticking coefficients for oxygen adsorption at various temperatures. For $T=300$ and 400 K, the impingement rate is 0.0002 ML/s. For $T=500$ K, the impingement rate is 1 ML/s.

This article is copyrighted as indicated in the article. Reuse of AIP content is subject to the terms at: http://scitation.aip.org/termsconditions. Downloaded to IP: 129.186.176.40 On: Tue, 19 Jan 2016 22:18:43

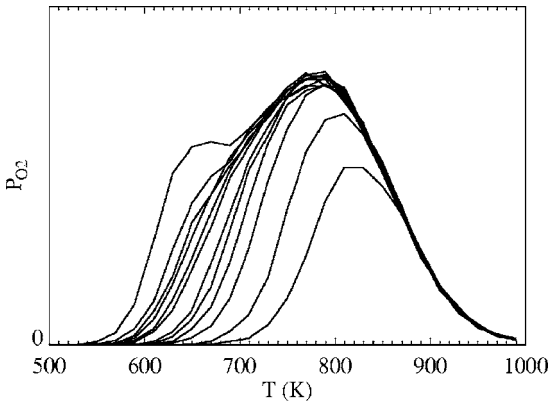

FIG. 9. Simulated TPD spectrum for oxygen desorption on Pd(100) for various O_2 exposure at 400 K. Exposure time is 0.1, 0.2, 0.4, 0.6, 0.8, 1, 2, 3, 6, 10, 20, and 50 s, with impingement rate at 1 ML/s and assuming an initial sticking coefficient of unity. Other conditions are the same as in Fig. 6.

vides a somewhat oversimplified description of the dissociative deposition dynamics for oxygen. Plausibly, there is a reduced but finite probability of sticking when one or more of the six 4fh sites neighboring the next NN 4fh adsorption sites is occupied by O. Likely, any NN pair of O thus formed would rapidly separate via thermal hopping. Second, when the oxygen coverage is around or above 0.5 ML, adsorption is not completely blocked as in our model. Instead, a $(\sqrt{5}\times\sqrt{5})R27°$ oxide structure emerges which involves Pd surface reconstruction. See Refs. 43 and 44 for recent investigations of this structure. Presently, substrate reconstruction has not been incorporated in our reaction model, but it is important for CO oxidation on Pd(100) at high pressure.[19] This regime will be the focus of our future research. Another factor is that real Pd substrates always have defects such as steps which limit the size of $p(2\times2)$ domains. This likely also leads to the enhancement of oxygen adsorption. In summary, due to these various factors, our modeling presumably somewhat underestimates the physical sticking coefficient.

Figure 9 shows results of TPD simulations for different oxygen exposures at 400 K. Consistently, experimental TPD spectra[45] show that the dominant peak shifts from above 800 K to around 750 K as oxygen exposure increases. An additional shoulder or peak around 650 K starts to emerge when the initial coverage of oxygen is above 0.25 ML. The latter reflects the influence of next NN repulsive O–O interactions, which lower the desorption barrier. This behavior in Fig. 9 is also seen in experiments. Figure 10 shows a snapshot of adlayer configuration at 620 K during TPD. We do not reproduce the very sharp peak for observed oxygen exposure over 30 L.[45,46] However, this sharp peak is due to the $(\sqrt{5}\times\sqrt{5})R27°$ phase mentioned above[47] which is not incorporated into our modeling.

As an aside, we mention that the TPD spectra in this and the previous section were calculated directly from KMC simulation of a LG model in which desorption rates are specified explicitly. A prominent alternative method for determining TPD spectra *assumes adlayer equilibration* and evaluates the desorption rate in terms of the adsorbate chemical potential and the sticking coefficient.[5] This method is

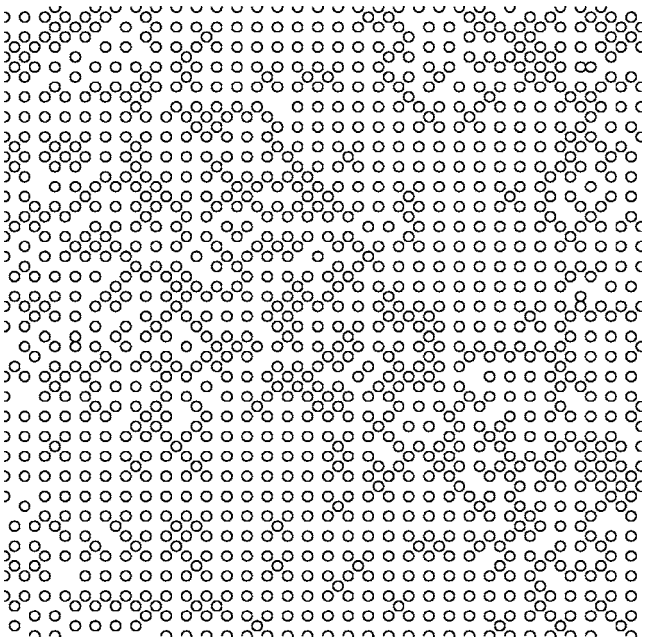

FIG. 10. Snapshot of the configuration of adsorbed oxygen at 620 K during a TPD simulation. The surface was initially exposed to 50 L of oxygen at 400 K.

appealing since determination of the chemical potential using the transfer matrix technique avoids potentially expensive simulations incorporating surface diffusion processes. One drawback, however, is that one must know the specific form for the coverage dependence of the sticking coefficient at the relevant desorption temperature. As shown earlier in Fig. 9, this form is sensitive to temperature, and it is typically not available at desorption temperature. Therefore, the utility of this approach for precisely predicting TPD spectra might be questioned. The assumption of equilibrium of chemisorbed phases during desorption is reasonable. However, there are certainly situations (e.g., surface oxide formation) where equilibrium is not achieved, as is demonstrated, e.g., by a dependence of the TPD spectrum on the deposition temperature.

VI. SIMULATION RESULTS FOR CO OXIDATION

A. Ordering of mixed CO+oxygen adlayer

As a prelude for our study of TPR and steady-state behavior for CO oxidation, it is instructive to briefly discuss the ordering within a mixed adlayer of CO and oxygen under conditions of limited reaction. We have already described the ordered structures formed by pure CO and by pure oxygen on the Pd(100) surface. Our selection of CO–CO and O–O adspecies interactions is made in part to ensure that our model recovers this experimentally observed ordering.[15,16] In principle, one can also utilize information about ordered structures formed within mixed adlayers to deduce lateral interactions between different types of adspecies. However, such information is quite limited, especially given the larger parameter space needed for a comprehensive analysis.

A two-stage deposition procedure is implemented in our simulations quite similar to that of titration experiments. However, the second stage of deposition, which produces the

This article is copyrighted as indicated in the article. Reuse of AIP content is subject to the terms at: http://scitation.aip.org/termsconditions. Downloaded to IP: 129.186.176.40 On: Tue, 19 Jan 2016 22:18:43

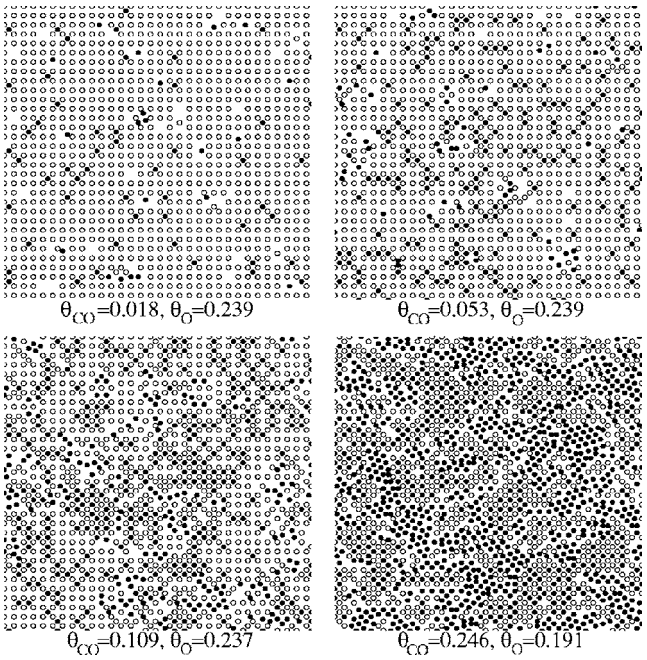

FIG. 11. Configurations of mixed CO and oxygen adlayers at 270 K. Open circles denote oxygen and closed circles denote CO.

mixed adlayer, is performed at a lower temperature where the reaction between CO and oxygen is insignificant (except in the later stages when the total coverage is high). Specifically, we first deposit an oxygen adlayer with $\theta_O=0.24$ ML at 400 K. As mentioned above, adsorbed oxygen forms a $p(2\times2)$ structure under these conditions. We then deposit CO at 270 K with a flux of 10^{-4} ML/s. Figure 11 shows typical configurations at various CO coverages. For $\theta_{CO}<0.1$ ML, CO mostly mixes into the oxygen adlayer which maintains its long-ranged $p(2\times2)$ order. When $\theta_{CO}>0.1$ ML, $c(2\times2)$ patches with higher oxygen coverage start to appear, leaving space in which CO can aggregate. Eventually, no $p(2\times2)$ regions remain, and the surface locally separates (i.e., locally entropically demixes) into $c(2\times2)$ oxygen patches and $c(2\sqrt{2}\times\sqrt{2})R45°$ CO patches.

This is qualitatively consistent with the LEED study of Stuve *et al.*[17] One difference is that in our model, local demixing only occurs when $T>250$ K (on time frame of about an hour), while Stuve *et al.* observed demixing occurring at temperatures as low as 80 K. This may due to the fact that our Metropolis algorithm for hopping of oxygen imposes a minimum diffusion barrier of 0.65 eV. This value is derived from experiments at low oxygen coverages. However, a more realistic algorithm for hopping might allow the diffusion barrier be significantly reduced at high CO and oxygen coverage, due to the effect of repulsive interactions. However, in this paper, we will not pursue such refinements since we mostly deal with high temperature behavior where such details are not likely to be crucial.

B. TPR spectra

TPR is a powerful technique for probing details of the reaction process. The presence of CO on the surface strongly inhibits oxygen adsorption. Thus, the typical experimental

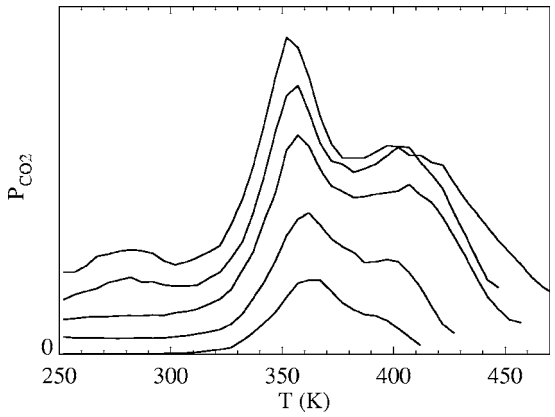

FIG. 12. Simulated TPR spectrum with heating rate 5 K s^{-1}. The initial coverage of oxygen is 0.252 ML, and the initial coverage of CO, from bottom to top, is 0.050, 0.099, 0.193, 0.279, and 0.396 ML.

procedure is to first expose the surface to some selected amount of oxygen, then to expose the oxygen-precovered surface to CO, and subsequently to monitor the reaction products while increasing the substrate temperature. We have performed simulations mimicking this experimental procedure. First, we dose the surface with 2.5 L of oxygen at 400 K, resulting in an oxygen coverage of about 0.25 ML. We then deposit various amounts of CO at 250 K. The temperature is subsequently raised at the rate of 5 K/s.

Figure 12 shows results for TPR spectra from our simulations. With a low initial CO coverage, there is just one reaction peak at around 360 K. As the initial CO coverage increases above 0.1 ML, another peak emerges actually at a higher temperature of about 400 K. With even higher CO coverage, a shoulder below 300 K also appears. These TPR features are associated with specific reaction scenarios: (i) the peak at 360 K is due to reaction involving a CO within the oxygen $p(2\times2)$ structure; (ii) the shoulder at 400 K is due to reaction between a CO outside an oxygen domain with peripheral oxygen, or between a CO and an isolated oxygen atom; and (iii) the lowest temperature state corresponds to reaction between a CO and an O at NN 4fh sites (with separation $d=a$).

We next elucidate the dependence of these features on CO coverage. The origin of the 360 K peak is clear. For low θ_{CO}, the amount of CO is insufficient to destroy the ordered oxygen $p(2\times2)$ structure. CO molecules are always within this ordered structure, where the reaction barrier is around 1.00 eV. A rather counterintuitive result in Fig. 12 is that increasing the initial CO coverage introduces a shoulder or peak in the TPR spectrum at a higher temperature. In contrast, in typical TPD experiments for adlayers with repulsive adspecies interactions, increasing initial coverage typically introduces lower temperature peaks. However, in our TPR study, introducing a sufficiently large amount of CO can destroy the ordered oxygen structure (either through repulsion, or by reacting away oxygen so that the amount of oxygen is not sufficient for maintaining ordering). Then after the initial peak at 360 K, the remaining CO and oxygen are disordered. In this situation, reaction between CO and oxygen have to overcome an additional barrier due to repulsive interaction between CO and oxygen of 0.19 eV. Thus the effective re-

This article is copyrighted as indicated in the article. Reuse of AIP content is subject to the terms at: http://scitation.aip.org/termsconditions. Downloaded to IP: 129.186.176.40 On: Tue, 19 Jan 2016 22:18:43

action activation energy is 1.19 eV. Introducing an even larger initial amount of CO leads to significant population of 4fh sites directly between adjacent O in the $p(2\times2)$ structure. Such CO reacts with a low barrier of 0.73 eV producing the low temperature peak.

The positions of the TPR peaks and their order of appearance (360 K, then 400 K, and finally 300 K, with increasing CO coverage) are consistent with experiments of Stuve *et al.*[17] The formation of a peak below 400 K and then emergence of a peak above 400 K with increasing CO coverage is also consistent with (but less clear in) the TPR spectra of Zheng and Altman.[18] There are some minor discrepancies between experiments and simulations, but also between the experiments themselves. In experiments for higher CO coverage, the peak at around 360 K does not change position much with increasing CO coverage. For our model, this peak position shifts slightly to lower temperatures as CO coverage increases. However, we have adopted a fairly simple prescription of the reaction barriers in our model (from many possible more complex choices), so this minor discrepancy is not surprising. It is worth noting that the broadness of TPR peaks is sensitive to how the reaction barriers depend on lateral interactions. On the other hand, the present model seems quite satisfactory when the total coverage is not much larger than 0.5 ML.

C. Reactive steady states and bistability

In this subsection, we study steady-state behavior of the reaction system under constant CO and oxygen pressure and for fixed temperature. As expected from traditional mean-field studies, for sufficiently low temperatures, our simulations reveal a range of CO partial pressures, where the system can either exist in a stable inactive or nearly CO-poisoned state (with little CO_2 production), or in a stable reactive state (with high CO_2 production). This regime of bistability disappears above a nonequilibrium critical point (in the temperature and CO partial-pressure plane), corresponding to a cusp bifurcation in traditional mean-field treatments.

There has been much interest in related nonequilibrium phase transitions and critical phenomena in idealized reaction models which usually incorporate limited adspecies mobility. In such models, simulation reveals a first-order phase transition at the partial pressure where the inactive and reactive states are equally stable.[48] The discontinuous transition disappears at a nonequilibrium critical point which is of the Ising type.[49,50] A constant-coverage simulation approach was proposed[51] which conveniently maps out the discontinuous variation of coverages with partial pressures. Loosely speaking, this approach is analogous to using a canonical rather than a grand canonical ensemble in equilibrium statistical physics. In the constant-coverage approach, one fixes either the CO or oxygen coverage (but not both) and lets the pressure change to maintain this prescribed coverage.

For realistic reaction models with rapid adspecies diffusion, the discontinuous transition is replaced by bistability.[52] The nonequilibrium critical point becomes of mean-field type rather than Ising type.[50] The constant-coverage simulation approach allows one to map out not just the stable steady states, but also the connecting unstable steady state.[52] These unstable states cannot be readily probed with conventional simulation techniques. Thus, in analyzing our LG model for CO oxidation on Pd(100), we utilize this constant-coverage simulation approach to provide the first steady-state bifurcation diagram for a realistic atomistic model of a surface reaction under UHV conditions.

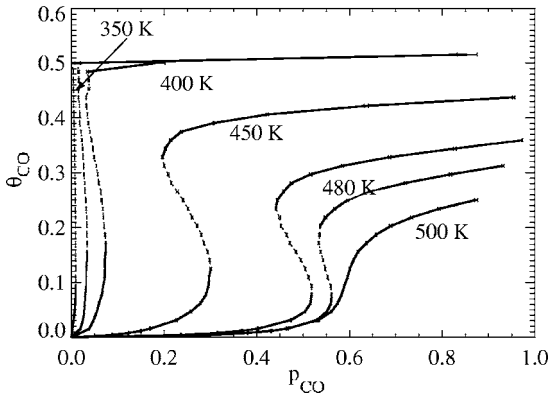

FIG. 13. Phase diagram showing behavior of the steady-state CO coverage for CO oxidation on Pd(100). The solid lines represent stable phases, while the dotted lines represent the unstable phase.

Figure 13 shows for different temperatures the variation of CO coverage with CO partial pressure, p_{CO}, in the stable and unstable steady states. Notice that bistability disappears at a critical temperature just below 500 K (although we caution that this value depends quite sensitively on the specification of CO desorption). Here, we have set the total flux of CO and oxygen to a fixed value of 1 ML/s. At relatively low temperatures, starting from the reactive steady state with low CO coverage (and high O coverage), as p_{CO} increases, CO coverage increases. Then at a certain pressure, the system will abruptly jump from the inactive state with high CO coverage and low oxygen coverage at the so-called upper spinodal point (where the reactive and unstable states merge and annihilate). Conversely, starting from an inactive state with high CO coverage at high CO pressure, as p_{CO} decreases, the system will jump to the reactive state with low CO coverage at the lower spinodal point (where the inactive and unstable states merge and annihilate). Such hysteresis behavior is commonly observed in experimental studies of CO oxidation.[1] The associated discontinuous jumps should not be (but often are) confused with the discontinuous transition in idealized reaction models with limited adspecies mobility.

Results for bistability from the above simulations can be presented more directly. Figure 14 shows the bistable region (shaded) in a T-p_{CO} bifurcation diagram. The boundaries of the bistable region correspond to the loci of the spinodal points. The bistable region terminates at higher temperatures at a cusp point. For high temperature or low CO partial pressure outside this region, only the reactive steady state exists. For low temperature or high CO partial pressure, only the inactive near CO-poisoned steady state exists.

Figure 15 shows snapshots of the system under the steady-state conditions at various temperatures and CO partial pressures. The pressures are chosen to be midway be-

This article is copyrighted as indicated in the article. Reuse of AIP content is subject to the terms at: http://scitation.aip.org/termsconditions. Downloaded to IP: 129.186.176.40 On: Tue, 19 Jan 2016 22:18:43

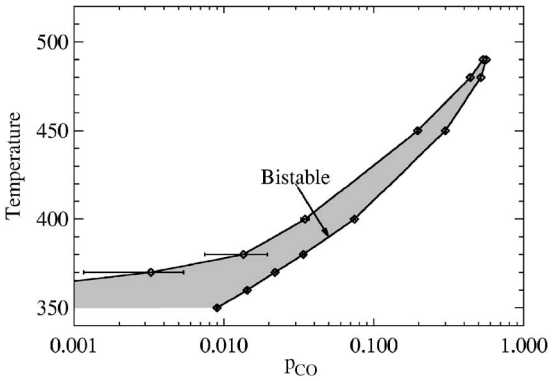

FIG. 14. Steady-state bifurcation diagram for CO oxidation on Pd(100). The shaded area represents the regime of bistability.

tween the upper and lower spinodal pressures. These are usually close to but not exactly at the equistability pressure where the two steady states are equally stable (in the sense that an interface between the two states is stationary).[22,52] Notice that as the temperature increases, the distinction between the inactive near CO-poisoned state and the reactive state diminishes. At the cusp point, the two states merge and become identical, resulting in critical fluctuations. An interesting feature is that for low temperatures, the oxygen adlayer in the reactive steady states has some long-range ordering. This has consequences for reaction front propagation in spatially nonuniform systems as it leads to significant reaction in the chemical diffusivity of CO. Some preliminary analysis has been published recently.[22]

VII. SUMMARY AND DISCUSSION

A long-standing goal of UHV surface science has been to provide a detailed understanding of catalytic surface reactions. Due to the complexity of these systems, there has been very little modeling based on a detailed and realistic atomistic description of the reaction process. Thus, here we were motivated to develop a realistic atomistic LG reaction model for CO oxidation on Pd(100) under UHV conditions. In addition to dependence on the kinetics of various processes, behavior of such a model is very sensitive to adlayer ordering which is controlled by the magnitude of weak adspecies interactions. Thus, considerable effort was expended to obtain precise values for the relevant energetic parameters. We combine information from both *ab initio* DFT calculations and statistical analysis of experimental observations. Extensive simulations are performed to directly confront a variety of standard surface science experiments. For the first time, we provide results for both TPR spectra and steady-state bifurcation behavior for CO oxidation under UHV conditions, which are based on an atomistic model rather than traditional phenomenological mean-field rate equations.

To a certain degree, this work represents a benchmarking effort to test the practicality and reliability of atomistic modeling of surface reaction systems, especially under UHV conditions. Thus, here we choose to model a classic surface reaction system, i.e., CO oxidation on Pd(100). A growing trend in such modeling is to exploit increasingly readily available tools for *ab initio* calculations for energetics. This applies in our study, although given current limitations of DFT, we also demand that the selected energetic parameters produce behavior consistent with TPD and ordering behavior observed in experimental studies of single-adspecies systems. With this multifaceted approach, satisfactory agreement with experiment has been achieved.

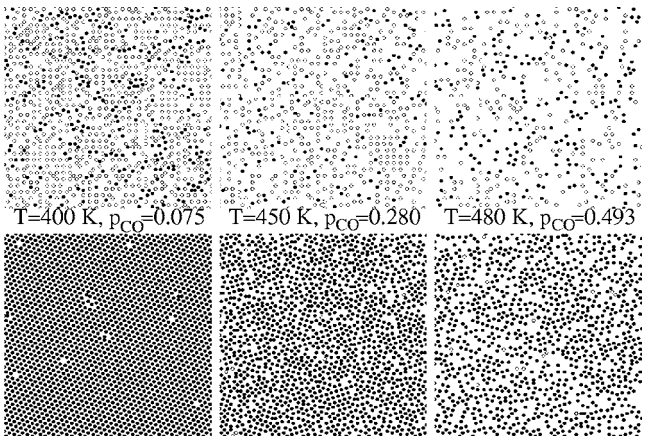

FIG. 15. Configuration of the mixed CO and oxygen adlayer in the steady states for CO oxidation on Pd(100) at various temperatures and CO partial pressures. The upper panel shows the reactive steady states and the lower panel shows the near CO-poisoned steady states.

ACKNOWLEDGMENTS

This work was supported by the Division of Chemical Sciences of the U.S. Department of Energy (Basic Energy Sciences). It was performed at Ames Laboratory which is operated for the U.S. DOE by Iowa State University under Contract No. W-7405-Eng-82.

APPENDIX: DEPENDENCE OF REACTIVE STEADY STATES ON DIFFUSION RATES

During CO oxidation under typical conditions, the atomistic process with by far the fastest rate is CO diffusion. For simulation of systems with a reasonable size and over an experimentally relevant period of time, it is usually not feasible to implement CO diffusion with the physically correct rate. Fortunately, some understanding is available of the dependence of reaction behavior on hopping rates. A well-defined hydrodynamic limit should be achieved as one systematically increases the hopping rates. However, it is important to determine how quickly this limit is attained. Figure 16 shows constant-coverage simulation results for the dependence on hopping rates of the steady-state CO coverage versus CO partial pressure. Specifically, for an "artificial" reference choice of equal hopping rates for CO and O, we show the dependence of steady-state behavior on the magnitude of the hopping rates (where all other rates are selected with their physical values at 400 K).

For low hopping rates, bistability is replaced by a first-order transition between reactive and inactive states (occurring at relatively high CO partial pressure). This transition corresponds to the pressure where these states are equistable. There is a weak metastable extension of the reactive (inactive) state above (below) this transition. As the hopping rate

This article is copyrighted as indicated in the article. Reuse of AIP content is subject to the terms at: http://scitation.aip.org/termsconditions. Downloaded to IP: 129.186.176.40 On: Tue, 19 Jan 2016 22:18:43

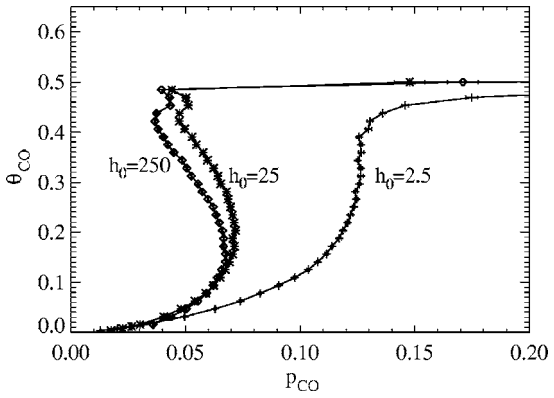

FIG. 16. Phase diagram for steady-state behavior of the CO coverage during CO oxidation at $T=400$ K with an "artificial" selection of hop rates. From right to left, $h_{CO}=h_O=0.25$, 2.5, 25, and 250 (in unit of hops per second). Results were obtained from Monte Carlo simulations using constant θ_{CO} algorithm.

increases, this weak metastability quickly develops into a robust bistability. The equistability point for the reactive and inactive states is not indicated in our plot. However, it usually occurs not far to the left of the upper spinodal, so it is clear that it shifts to lower pressures with increasing hop rate. However, most of this shift occurs quickly as hop rates increase from small values. Thus, for $h_0=25/s$, the system is already close to the hydrodynamic limit (as is clear by comparing behavior with that for $h_0=250/s$).

[1] R. Imbihl, Prog. Surf. Sci. **44**, 185 (1993).
[2] T. Engel and G. Ertl, Adv. Catal. **28**, 1 (1979).
[3] W. H. Weinberg, Annu. Rev. Phys. Chem. **34**, 217 (1983).
[4] A. Patrykiejew, S. Sokołowski, and K. Binder, Surf. Sci. Rep. **37**, 207 (2000).
[5] H. J. Kreuzer and S. H. Payne, in *Equilibria and Dynamics of Gas Adsorption on Heterogeneous Solid Surface*, Studies in Surface Science and Catalysis Vol. 104, edited by W. Rudziński, W. A. Steele, and G. Zgrablich (Elsevier, Amsterdam, 1997), p. 153.
[6] B. Meng and W. H. Weinberg, Surf. Sci. **374**, 443 (1997).
[7] A. P. J. Jansen, Phys. Rev. B **69**, 035414 (2004).
[8] C. Stampfl, H. J. Kreuzer, S. H. Payne, H. Pfnür, and M. Scheffler, Phys. Rev. Lett. **83**, 2993 (1999).
[9] C. G. M. Hermse, F. Frechard, A. P. van Bavel, J. J. Lukkien, J. W. Niemantsverdriet, R. A. van Santen, and A. P. J. Jansen, J. Chem. Phys. **118**, 7081 (2003).
[10] E. W. Hansen and M. Neurock, Surf. Sci. **464**, 91 (2000).
[11] D. A. Walthall, S. Chopra, and M. Neurock (unpublished).
[12] K. Reuter, D. Frenkel, and M. Scheffler, Phys. Rev. Lett. **93**, 116105 (2004).
[13] K. J. Caspersen, A. R. Layson, C. R. Stoldt, V. Fournee, P. A. Thiel, and J. W. Evans, Phys. Rev. B **65**, 193407 (2002).
[14] S. Völkening and J. Wintterlin, J. Chem. Phys. **114**, 6382 (2001); N. V. Petrova and I. N. Yakovkin, Surf. Sci. **578**, 162 (2005).
[15] D.-J. Liu, J. Chem. Phys. **121**, 4352 (2004).
[16] D.-J. Liu and J. W. Evans, Surf. Sci. **563**, 13 (2004).
[17] E. M. Stuve, R. J. Madix, and C. R. Brundle, Surf. Sci. **146**, 155 (1984).
[18] G. Zheng and E. I. Altman, J. Phys. Chem. B **106**, 1048 (2002).
[19] B. L. M. Hendriksen, S. C. Bobaru, and J. W. M. Frenken, Surf. Sci. **552**, 229 (2004).
[20] A. Eichler and J. Hafner, Phys. Rev. B **57**, 10110 (1998).
[21] C. J. Zhang and P. Hu, J. Am. Chem. Soc. **123**, 1166 (2001).
[22] D.-J. Liu and J. W. Evans, Phys. Rev. B **70**, 193408 (2004).
[23] G. Kresse and J. Hafner, Phys. Rev. B **47**, R558 (1993).
[24] G. Kresse and J. Furthmüller, Phys. Rev. B **54**, 11169 (1996).
[25] J. P. Perdew, K. Burke, and M. Ernzerhof, Phys. Rev. Lett. **77**, 3865 (1996).
[26] G. Kresse and D. Joubert, Phys. Rev. B **59**, 1758 (1999).
[27] D. A. King and M. G. Wells, Proc. R. Soc. London, Ser. A **339**, 245 (1976).
[28] C. R. Brundle, R. J. Behm, and J. A. Barker, J. Vac. Sci. Technol. A **2**, 1038 (1984).
[29] S.-L. Chang and P. A. Thiel, Phys. Rev. Lett. **59**, 296 (1987).
[30] J. W. Evans, J. Chem. Phys. **87**, 3038 (1987).
[31] R. J. Behm, K. Christmann, G. Ertl, and M. A. Van Hove, J. Chem. Phys. **73**, 2984 (1980).
[32] P. J. Feibelman, B. Hammer, J. K. Nørskov, F. Wagner, M. Scheffler, R. Stumpf, R. Watwe, and J. Durnesic, J. Phys. Chem. B **105**, 4018 (2001).
[33] S. E. Mason, I. Grinberg, and A. M. Rappe, Phys. Rev. B **69**, 161401(R) (2004).
[34] A. M. Bradshaw and F. M. Hoffmann, Surf. Sci. **72**, 513 (1978).
[35] F. M. Hoffmann, Surf. Sci. Rep. **3**, 107 (1983).
[36] J. Szanyi and D. Goodman, J. Phys. Chem. **98**, 2972 (1994).
[37] Y. Y. Yeo, L. Vattuone, and D. A. King, J. Chem. Phys. **106**, 1990 (1997).
[38] S. Renisch, R. Schuster, J. Wintterlin, and G. Ertl, Phys. Rev. Lett. **82**, 3839 (1999).
[39] V. P. Zhdanov, Surf. Sci. Rep. **12**, 183 (1991).
[40] D.-J. Liu and J. W. Evans, Multiscale Model. Simul. **4**, 424 (2005).
[41] A. Cassuto and D. A. King, Surf. Sci. **102**, 388 (1981).
[42] A. Gross, S. Wilke, and M. Scheffler, Surf. Sci. **357–358**, 614 (1996).
[43] M. Saidy, O. L. Warren, P. A. Thiel, and K. A. Mitchell, Surf. Sci. **494**, L799 (2001).
[44] M. Todorova, E. Lundgren, V. Blum *et al.*, Surf. Sci. **541**, 101 (2003).
[45] S.-L. Chang and P. A. Thiel, J. Chem. Phys. **88**, 2071 (1988).
[46] G. Zheng and E. I. Altman, Surf. Sci. **504**, 253 (2002).
[47] S.-L. Chang, P. A. Thiel, and J. W. Evans, Surf. Sci. **205**, 117 (1988).
[48] R. M. Ziff, E. Gulari, and Y. Barshad, Phys. Rev. Lett. **56**, 2553 (1986).
[49] T. Tomé and R. Dickman, Phys. Rev. E **47**, 948 (1993).
[50] D.-J. Liu, N. Pavlenko, and J. W. Evans, J. Stat. Phys. **114**, 101 (2004).
[51] R. M. Ziff and B. J. Brosilow, Phys. Rev. A **46**, 4630 (1992).
[52] J. W. Evans, D.-J. Liu, and M. Tammaro, Chaos **12**, 131 (2002).

This article is copyrighted as indicated in the article. Reuse of AIP content is subject to the terms at: http://scitation.aip.org/termsconditions. Downloaded to IP: 129.186.176.40 On: Tue, 19 Jan 2016 22:18:43